A Photometric Study of the Eclipsing Binary Star V958 Monocerotis

Edward J. Michaels
Stephen F. Austin State University, Department of Physics and Astronomy, P.O. Box 13044, Nacogdoches, TX 75962; emichaels@sfasu.edu

Received April 30, 2016; revised May 24, 2016; accepted June 7, 2016

Abstract Presented are new precision multi-band observations for the eclipsing binary V958 Mon. The orbital period is less than 0.3 day and the light curves exhibit total eclipses. A new ephemeris was determined and a simultaneous four-color light curve solution was obtained with the Wilson-Devinney program. The geometric and photometric elements derived are consistent with a W-type contact binary.

1. Introduction

The Northern Sky Variability Survey (NSVS) has provided a wealth of new variable star discoveries, many of which are W Ursae Majoris contact binaries (Wozniak *et al.* 2004). From this survey V958 Mon was first identified as an EW/KW-type eclipsing binary by Otero *et al.* (2004). It was also found in NSVS data by an automated variable star classification technique (Hoffman *et al.* 2009). A photometric orbital period of P = 0.29829 day was reported. The Large Sky Area Multi-Object Fiber Spectroscopic Telescope (LAMOST) survey gives an effective temperature for V958 Mon of T_{eff} = 4990 K, a metallicity of [Fe/H] = –0.02, a heliocentric radial velocity of V_r = –34.31 km/sec, and surface gravity of log g = 4.115 (cgs) (Luo *et al.* 2015). One time of minimum light was observed by Diethelm (2011) and second one by Nelson (2011). In Zejda *et al.*'s (2012) *Catalogue of Variable Stars in Open Cluster Fields*, V958 Mon is listed as a member of the nearby galactic cluster Platais 6 (HIP 29713). The distance to this cluster is 348 pc (Kharchenko *et al.* 2005).

In this paper a photometric study of V958 Mon is presented. It is organized into three sections. The observations and data reduction techniques are presented in section 2. New times of minima and a period analysis are presented in section 3. Light curve analysis using BINARY MAKER 3.0 (BM) and the Wilson-Devinney (WD) model is presented in section 4. Discussion and conclusions are presented in section 5.

2. Observations

Photometric observations were made using an SBIG-STXL camera with a cooled KAF-6303E CCD (–30°C) and the 0.31-m Ritchey-Chrétien robotic telescope of the Waffelow Creek Observatory (http://obs.ejmj.net/index.php). Images were acquired in each of four passbands on the following nights in 2015: December 2, 3, 4, 5, and 6. A total of 1,855 images were obtained: 531 in Johnson V, 443 in Sloan g', 442 in Sloan r', and 439 in Sloan i'. This set of data was used in the light curve analysis of section 4 of this paper. Additional Johnson B and V images had also been acquired earlier in 2015 (February 8, 9, 10, 11, 12, 13, 17, and 18) for determining new times of minima. All images were calibrated with bias, dark, and flat field frames. MIRA software (Mirametrics 2015) was used for calibration and ensemble differential aperture photometry.

The seven comparison stars (C1–C7) and the check (K) star used in this study are listed in Table 1 with a finder chart shown in Figure 1. The standard magnitudes for each of these stars was taken from the AAVSO Photometric All-Sky Survey (APASS; Henden *et al.* 2014). The instrumental magnitudes of V958 Mon were converted to standard magnitudes using these comparison stars. The time for each observation was converted to orbital phase using:

$$\Phi = \frac{T - T_0}{P} - \mathrm{Int}\left(\frac{T - T_0}{P}\right) \quad (1)$$

where T is the Heliocentric Julian Date of the observation, T_0 is a time of minimum for a primary eclipse (epoch), and P is the orbital period. Throughout this paper the values used for epoch and period are T_0 = 2457363.715748 and P = 0.29830597 day (see section 3.1). All light curves are plotted from phase –0.6 to 0.6 with negative orbital phase defined as Φ – 1. Figure 2 shows the folded light curves for each passband in standard magnitudes. In the bottom panel of Figure 2 are the Johnson V standard magnitudes for the K star. For each night a plot of the K star magnitudes for each passband was inspected and no significant variability was detected. All the observations in this study are available from the AAVSO International Database (Kafka 2015).

On one night of excellent seeing, December 6, it was discovered that V958 Mon has a close companion star. The star is located approximately 4.0 ± 0.1 arcsec from V958 Mon at a position angle of 338 ± 2 degrees. All photometry was performed with an aperture size that included both stars since on most nights the stars were not resolved. To measure the approximate light contribution from the companion star, a separate data reduction was performed for the December 6 observations using a smaller aperture that excluded the companion's light. Using the smaller aperture the peak magnitude at phase 0.25 was differenced with the peak magnitude using the larger aperture which included both stars. The magnitude differences for each passband provided the initial starting values for third light in the WD model of section 4.

3. Analysis

3.1. Period determination

The initial ephemeris used in this study was taken from Otero *et al.* (2004) and is given by:

Table 1. Stars used in this study.

Star	R.A. (2000) h m s	Dec. (2000) ° ′ ″	V	g′	r′	i′
V958 Mon	06 22 58	+04 28 18				
[1]GSC 0140-0872 (C1)	06 22 30	+04 19 11	11.708 ± 0.036	12.322 ± 0.021	11.243 ± 0.050	10.787 ± 0.057
[1]GSC0140-1016 (C2)	06 21 17	+04 34 54	11.826 ± 0.043	11.973 ± 0.037	11.695 ± 0.059	11.615 ± 0.064
[1]GSC 0140-0737 (C3)	06 21 41	+04 36 44	12.147 ± 0.025	12.224 ± 0.022	12.093 ± 0.041	12.127 ± 0.040
[1]GSC 0140-0615 (C4)	06 22 14	+04 21 29	12.295 ± 0.057	12.965 ± 0.025	11.814 ± 0.030	11.291 ± 0.049
[1]GSC 0141-1058 (C5)	06 22 42	+04 25 54	12.416 ± 0.040	12.572 ± 0.014	12.300 ± 0.053	12.263 ± 0.031
[1]GSC 0140-1059 (C6)	06 22 06	+04 29 51	12.549 ± 0.032	13.180 ± 0.027	12.063 ± 0.034	11.562 ± 0.049
[1]GSC 0140-1171 (C7)	06 22 10	+04 23 24	12.567 ± 0.036	13.448 ± 0.023	11.856 ± 0.041	11.116 ± 0.043
[2]GSC 0140-1153 (K)	06 22 10	+04 35 10	12.743 ± 0.040	12.909 ± 0.014	12.626 ± 0.039	12.588 ± 0.042
[3]Observed check star magnitudes (K)			12.744 ±0.010	12.934 ± 0.010	12.631 ± 0.012	12.566 ± 0.013

APASS [1]comparison stars (C1–C7) and [2]check (K) star magnitudes and errors. The observed [3]check star magnitudes are the averages over all nights for each passband.

HJD Min I = 2451525.891 + 0.298305 E. (2)

Using the Kwee and van Woerden (1956) method, eight new times of minima were determined from the observations. These minima and two others found in the literature are reported in Table 2. A new linear ephemeris was determined by least-squares solution and is given by:

HJD Min I = 2457363.7158 (15) + 0.29830597 (8) E. (3)

This ephemeris should be useful for predicting future minima times. Figure 3 shows the O-C diagram from Equation 3.

3.2. Temperature, spectral type

The temperature of the cooler secondary star was determined from the (g'–r') color index at primary minimum (Φ = ±0.025). Since the minimum is a total eclipse, only light from the secondary star is measured at this orbital phase. All g' and r' observations were binned with a phase width of 0.01. Both phase and magnitude were averaged in each bin interval. The binned r' magnitudes were subtracted from the linearly interpolated binned g' magnitudes which gives a (g'–r') color of 0.724 ± 0.022 at primary minimum. Figure 4 shows the binned r' magnitude light curve and the bottom panel the color index. The (g'–r') color was transformed to (B–V) using Bilir's (2005) transformation equation,

$$(B-V) = \frac{(g' - r') + 0.252}{1.124}. \quad (4)$$

This gives an observed color index of (B–V) = 0.868 ± 0.020. The color excess for this star is likely very small. V958 Mon lies approximately along the same line of sight as the Platais 6 cluster and is also somewhat closer than the cluster. The measured color excess for the cluster is E(B–V) = 0.000 (Kharchenko *et al.* 2005) which means the reddening for V958 Mon is probably quite small. Using Table 5 of Pecaut and Mamajek (2013) gives an effective temperature of T_{eff} = 5111 ± 57K for the secondary star. This temperature compares well with the LAMOST value of 4990 K.

3.3. Synthetic light curve modeling

The light curves were analyzed using BINARY MAKER 3.0 (BM3) (Bradstreet and Steelman 2002) and the WD program (Wilson and Devinney 1971; Van Hamme and Wilson 1998). The observations were binned in both phase and magnitude with a phase interval of 0.01. On average each binned data point was formed by four observations. The binned magnitudes were then converted to relative flux for light curve modeling. BM3 was used to make the initial synthetic light curve fit to each observed light curve using standard convective parameters and limb darkening coefficients from Van Hamm's (1993) tabular values. The parameters resulting from the initial fits to each light curve were averaged. These averages were used as the input values for the computation of a simultaneous 4-color light curve solution with the WD program. The weight given to each input data point was set to the number of observations that formed the point. Mode 3 was set in the program since the light curves are typical of a short-period contact binary with the flat bottoms of both minima indicating total eclipses. The Kurucz stellar atmosphere model was used and logarithmic limb darkening coefficients were calculated by the program. The Method of Multiple Subsets (MMS) was employed to minimize strong correlations of the parameters (Wilson and Biermann 1976). The fixed inputs included standard convective parameters: gravity darkening, $g_1 = g_2 = 0.32$ (Lucy 1968), albedo value $A_1 = A_2 = 0.5$ (Ruciński 1969), and the effective temperature of the cooler star, T_2, was set to the value of 5111K determined in section 3.2. The solution's adjustable parameters include the

Table 2. Available times of minima and O–C residuals from Equation 3.

Epoch HJD 2400000+	*Error*	*Cycle*	*O-C Linear*	*References*
55588.6470	0.0003	13619.5	0.00094	Nelson 2011
55907.8323	0.0003	14689.5	–0.00115	Diethelm 2011
57065.7080	0.0001	18571.0	–0.00011	this paper
57066.6032	0.0001	18574.0	0.00015	this paper
57071.6742	0.0001	18591.0	0.00000	this paper
57359.8379	0.0001	19557.0	0.00013	this paper
57360.7327	0.0002	19560.0	0.00001	this paper
57361.7766	0.0002	19563.5	–0.00012	this paper
57362.8209	0.0002	19567.0	0.00008	this paper
57363.7158	0.0002	19570.0	0.00007	this paper

inclination (i), mass ratio ($q = M_2 / M_1$), potential ($\Omega, \Omega_1 = \Omega_2$), temperature of the primary star (T_1), the normalized flux for each wavelength (L), and third light (l). The best-fit solution is shown in column 2 of Table 3. The parameters with formal errors are the adjusted ones with the subscripts 1 and 2 referring to the primary and secondary stars being eclipsed at Min I and Min II, respectively. The fill-out parameter was calculated by BM3. It is defined by:

$$f = \frac{\Omega_{inner} - \Omega}{\Omega_{inner} - \Omega_{outer}}, \quad (5)$$

where Ω_{inner} and Ω_{outer} are the inner and outer critical equipotential surfaces and Ω is the equipotential surface that describes the stellar surface (Lucy and Wilson 1979). The third light in the solution is the percent of light contributed at an orbital phase of 0.25 by a nearby field star (see section 2). The normalized light curves for each passband overlaid by the synthetic solution curves (solid lines) are shown in Figure 5, with the residuals shown in Figure 6.

3.4. Spot model

The asymmetries often seen in eclipsing binary light curves are usually attributed to large cool spots, hot regions such as faculae, or gas streams that impact one of the stars. The light curves of V958 Mon show no obvious O'Connell effect but excess light was noted in the residual curves on either side of secondary eclipse (Figure 6). To fit the asymmetries in the light curves, a second solution was attempted by adding an over-luminous spot to the larger star. Since the excess light was reasonably symmetric about secondary minimum, the spot should be located along or close to the line of centers between the two stars either above or below the contact region. Both of these spot locations were modeled with BM3 by adjusting each spots parameters (latitude, longitude, spot size, and temperature) until a good fit was obtained between the synthetic and observed light curves. Both spot positions produced almost equally good fits. The spot modeled below the contact region had a marginally better fit, therefore its parameters were included in a new WD solution attempt. The stellar parameters from the first solution were held fixed while the spot parameters were adjusted until the solution converged. The spot parameters were then held fixed and the stellar parameters adjusted until the solution converged again. This process was repeated until the model converged to a final solution. The final values for the spotted solution parameters are shown in column 3 of Table 3. Figure 7 shows the spotted model fits (solid lines) to the observed light curves and Figure 8 shows the residuals. The differences between the stellar parameters for each model (spotted and unspotted) are very small. The sum of the residuals squared for the spotted solution was 0.013 and 0.023 for the unspotted model (1.8 times larger). A graphical representation of the spotted solution is shown in Figure 9.

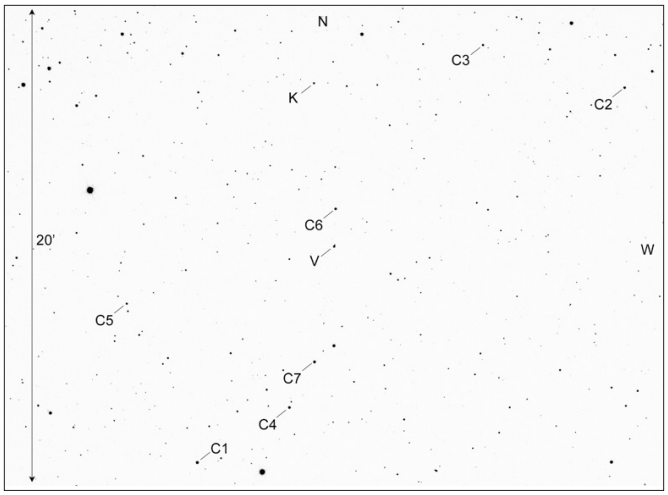

Figure 1. Finder chart for V958 Mon (V), comparison (C1–C7), and check (K) stars.

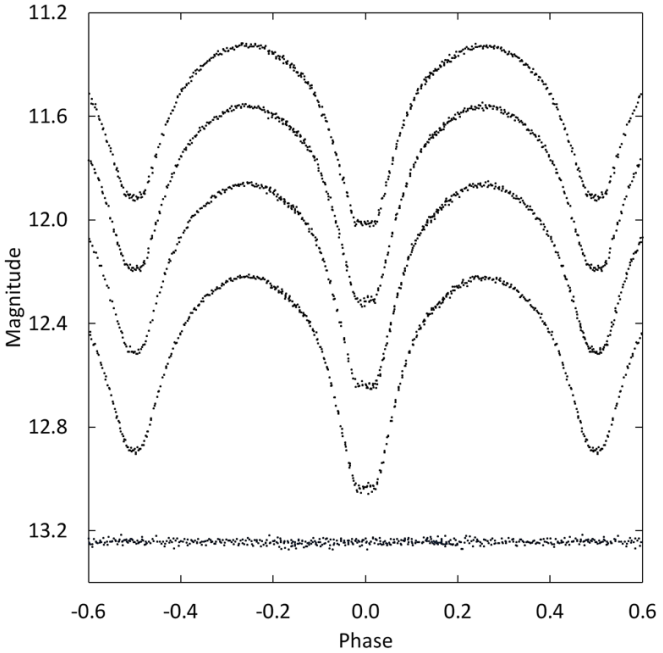

Figure 2. Folded light curves for each observed passband. The differential magnitudes of the variable were converted to standard magnitudes using the calibrated magnitudes of the comparison stars. From top to bottom the light curve passbands are Sloan i', Sloan r', Johnson V, Sloan g'. The bottom curve shows the Johnson V magnitudes of the check star (offset +0.5 magnitude). The standard deviations of check star magnitudes (all nights) are shown in Table 1. Error bars are not shown for clarity.

Table 3. V958 Mon synthetic light curve solutions.

parameter	*Solution (no spots)*	*Solution (with spot)*
phase shift	0.0002 ± 0.0001	0.0003 ± 0.0001
i (°)	86.4 ± 0.4	86.4 ± 0.4
T_1 (K)	5465 ± 3	5465 ± 2
T_2 (K)	5111*	5111*
$\Omega_1 = \Omega_2$	5.489 ± 0.026	5.489 ± 0.026
$q(M_2 / M_1)$	2.253 ± 0.018	2.250 ± 0.019
filling factor	19%	19%
$L_1 / (L_1 + L_2)$ (B)	—	—
$L_1 / (L_1 + L_2)$ (V)	0.4100 ± 0.0007	0.4101 ± 0.0004
$L_1 / (L_1 + L_2)$ (g')	0.4242 ± 0.0007	0.4243 ± 0.0006
$L_1 / (L_1 + L_2)$ (r')	0.3973 ± 0.0007	0.3974 ± 0.0005
$L_1 / (L_1 + L_2)$ (i')	0.3864 ± 0.0006	0.3864 ± 0.0004
l_3 (V)**	0.0112 ± 0.0042	0.0121 ± 0.0042
l_3 (g')	0.0244 ± 0.0042	0.0262 ± 0.0042
l_3 (r')	0.0183 ± 0.0044	0.0198 ± 0.0043
l_3 (i')	0.0362 ± 0.0043	0.0375 ± 0.0043
r_1 side	0.3120 ± 0.0009	0.3103 ± 0.0007
r_2 side	0.4703 ± 0.0036	0.4884 ± 0.0039
spot parameters		
colatitude (°)	—	113 ± 2
longitude (°)	—	356 ± 1
spot radius (°)	—	12 ± 2
temp.- factor	—	1.17 ± 0.04

** Assumed. ** Third lights are the percent of light contributed at orbital phase 0.25.*

Table 4. Stellar parameters for V958 Mon.

Parameter	*Symbol*	*Value*
Stellar masses	M_1 ($M_\odot$)	0.43 ± 0.06
	M_2 ($M_\odot$)	0.98 ± 0.06
Semi-major axis	a ($R_\odot$)	2.11 ± 0.01
Mean stellar radii	R_1 ($R_\odot$)	0.68 ± 0.01
	R_2 ($R_\odot$)	0.98 ± 0.02
Stellar luminosity	L_1 ($L_\odot$)	0.38 ± 0.05
	L_2 ($L_\odot$)	0.59 ± 0.07
Bolometric magnitude	$M_{bol,1}$	5.82 ± 0.06
	$M_{bol,2}$	5.33 ± 0.09
Surface gravity	log g_1 (cgs)	4.41 ± 0.06
	log g_2 (cgs)	4.45 ± 0.03
Mean density	$\overline{\rho}_1$ (g cm^{-3})	1.91 ± 0.10
	$\overline{\rho}_2$ (g cm^{-3})	1.46 ± 0.08

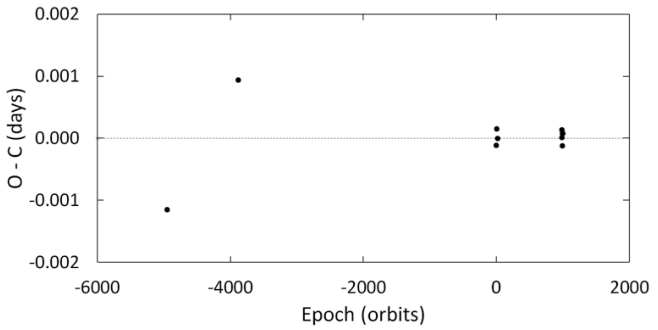

Figure 3. O–C residuals from linear ephemeris fit of Equation (3).

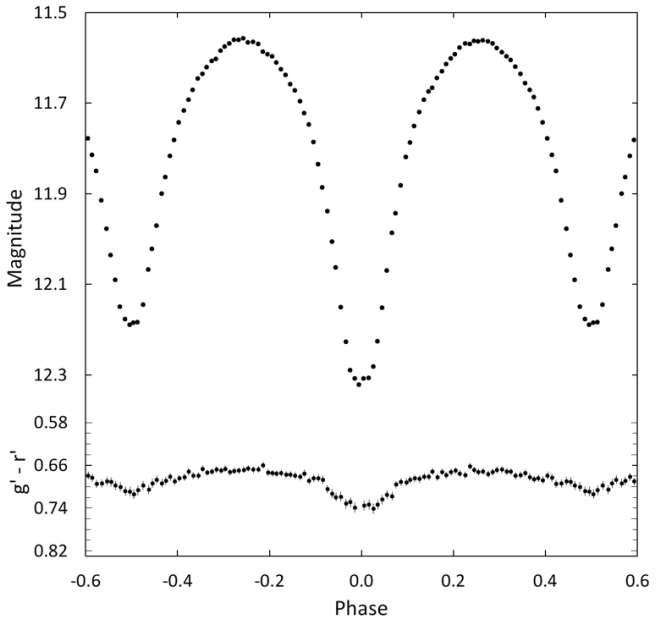

Figure 4. Light curve of all r'-band observations in standard magnitudes (top panel). The observations were binned with a phase width of 0.01. The errors for each binned point are about the size of the plotted points. The g'–r' colors (botttom panel) were calculated by subtracting the binned Sloan g' magnitudes from the linearly interpolated binned Sloan r' magnitudes.

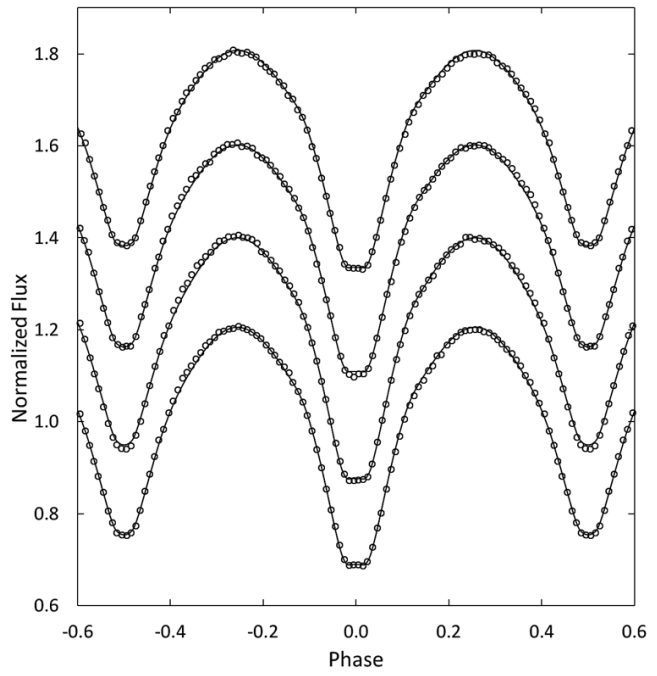

Figure 5. The WD model fit without spots (solid curve) to the observed normalized flux curves for each passband. From top to bottom the passbands are Sloan i', Sloan r', Johnson V, and Sloan g'. Each curve is offset by 0.2 for this combined plot. The best-fit parameters are given in column 2 of Table 3. Error bars are omitted from the points for clarity.

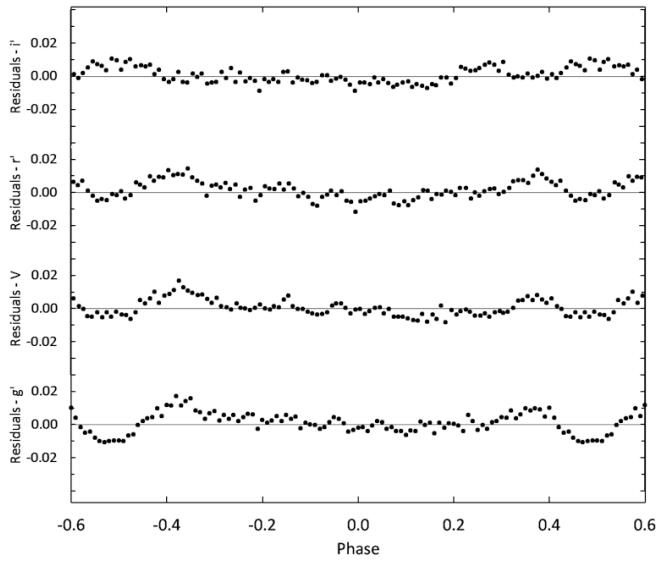

Figure 6. The residuals for the best-fit WD model without spots. Error bars are omitted from the points for clarity.

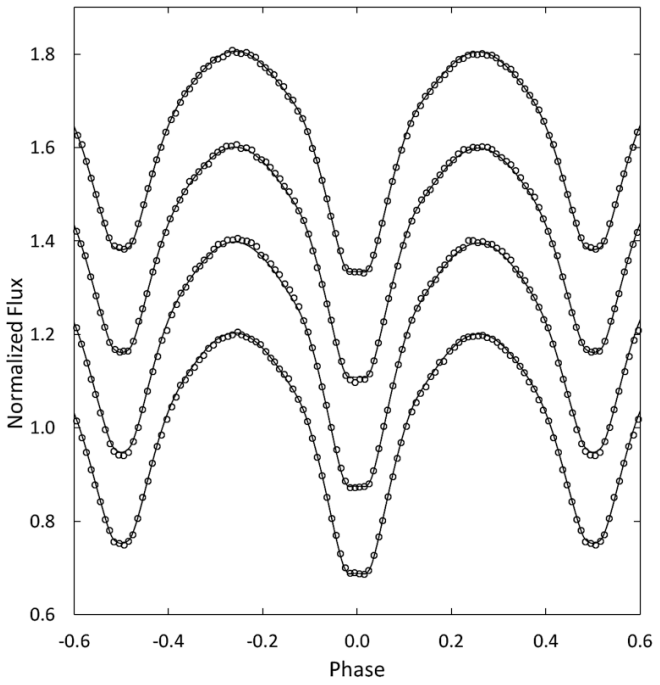

Figure 7. The WD model fit with spots (solid curve) to the observed normalized flux curves for each passband. From top to bottom the passbands are Sloan i', Sloan r', Johnson V, and Sloan g'. Each curve is offset by 0.2 for this combined plot. The best-fit parameters are given in column 3 of Table 3. Error bars are omitted from the points for clarity.

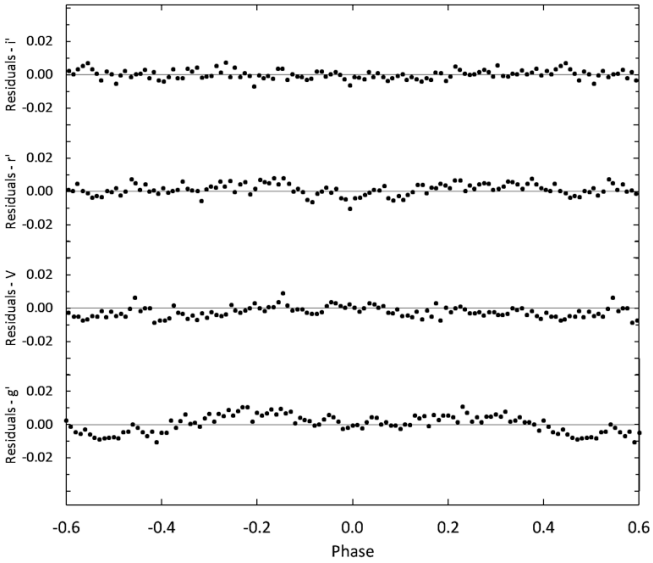

Figure 8. The residuals for the spotted WD model in each passband. Error bars are omitted from the points for clarity.

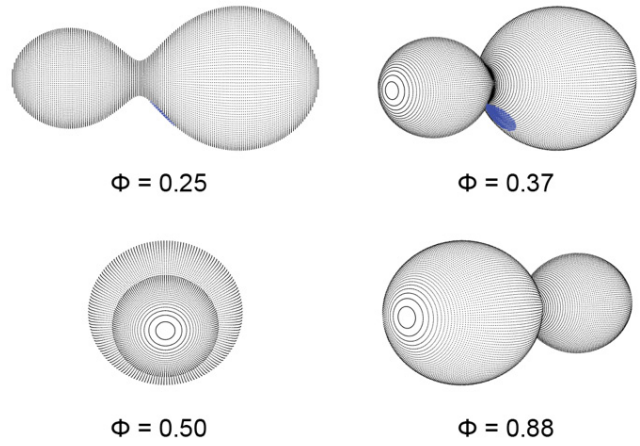

Figure 9. Roche Lobe surfaces of the best-fit WD spot model with orbital phase shown below each diagram.

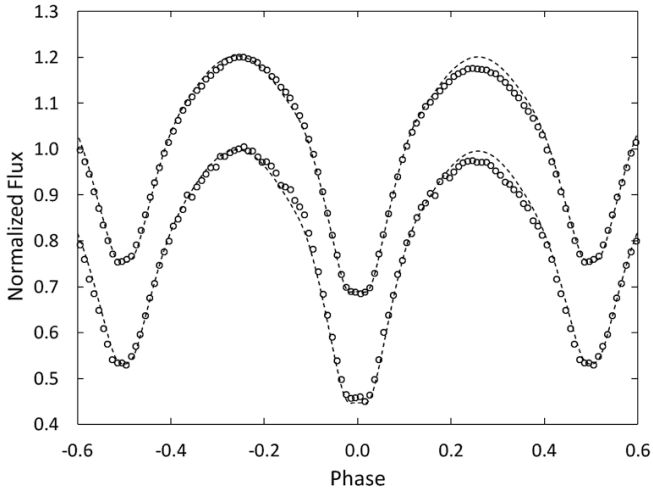

Figure 10. The WD model without spots overlaid (dashed curve) onto the February 2015 Johnson BV normalized flux curves. Johnson V is the top curve (offset by 0.2) and Johnson B the bottom. Error bars are omitted from the points for clarity.

4. Discussion and conclusions

W-type eclipsing binaries of W UMa type most often consist of two cool stars in contact whose spectral types are F, G, or K and whose components have nearly equal surface temperatures in spite of their often greatly differing masses. This study confirms that V958 Mon is a member of the W-type subclass where the larger more massive star is cooler and has less surface brightness than its companion and primary minimum is an occultation. The best-fit WD solution with a fill-out value of 19% is consistent with a contact binary. Given the total eclipses observed, the derived parameters should have good accuracy, as shown by Wilson (1978) and Terrell and Wilson (2005). The stellar parameters can now be determined for each star. From Qian's (2003) statistical study of contact systems the mass of the larger cooler star is given by:

$$M_2 = 0.391\ (\pm 0.059) + 1.96\ (\pm 0.17)\ P\ , \qquad (6)$$

where P is the orbital period. This equation gives the secondary star's mass, $M_2 = 0.98 \pm 0.06\ M_\odot$, and combined with the mass ratio gives the primary star's mass, $M_1 = 0.43 \pm 0.06\ M_\odot$. Applying Kepler's Third Law gives the distance between the stars' mass centers, $2.11 \pm 0.01\ R_\odot$. Mochnacki (1981) showed the mean stellar densities for contact binaries are given by:

$$\overline{\rho}_1 = \frac{0.0189}{r_1^3\ (1 + q)\ P^2} \text{ and } \overline{\rho}_2 = \frac{0.0189q}{r_2^3\ (1 + q)\ P^2}\ , \qquad (7)$$

where the stellar radius is normalized to the semi-major axis and P is in days. The computed values are $\overline{\rho}_1 = 1.91\ g\,cm^{-3}$ and $\overline{\rho}_2 = 1.46\ g\,cm^{-3}$. The stellar radii, surface gravities, luminosities, and bolometric magnitudes were calculated by the Wilson and Devinney (1971) light curve program (LC). All the absolute stellar parameters are presented in Table 4.

The light curves shown in Figure 2 have equal maxima but Johnson V-band and B-band observations taken 11 months earlier displayed a noticeable O'Connell effect. This can be seen in Figure 10, which shows the B and V light curves overlaid with the WD solution without spots (dashed line). For the V-band light curve, the maximum at orbital phase 0.25 was 0.15 magnitude fainter than the maximum at phase 0.75. These changes in the light curves are most likely the result of changing spot configurations. This is an indication of magnetically active stars which are often found in short period low-mass contact binaries such as V958 Mon.

A distance estimate to V958 Mon can be made using Ruciński and Duerbeck's (1997) luminosity calibration for contact binaries that is based on HIPPARCOS parallaxes. This empirical relationship is given by:

$$M_v = -4.44 \log_{10}(P) + 3.02\ (B-V)_o + 0.12\ . \qquad (8)$$

Substituting into Equation 8 the orbital period and the observed (B–V) color index gives an absolute magnitude of $M_V = 5.07 \pm 0.22$. Using the apparent V-magnitude at quadrature, $m_V = 11.861 \pm 0.005$, gives a distance modulus of $(m - M)_V = 6.79 \pm 0.22$ and an estimated distance of 228 ± 23 pc. A correction for interstellar extinction was not applied due to the very small color excess for this star (see section 3.2).

A spectroscopic study of V958 Mon would be invaluable in confirming the absolute parameters of the component stars presented here. This star should be patrolled frequently. Several years of new minima times will be necessary to determine if any orbital period change is occurring. Period changes can result from magnetic braking, conservative mass exchange between the stars, or orbital motion about a third body. Lastly, V958 Mon does not appear to be a member of the Platais 6 cluster. Platais 6 is a very young cluster with an age of 60.3 Myr (Wu *et al.* 2009). When W UMa stars evolve to the beginning of their contact phase, they can range in age from 4.8 to 12.5 Gyr (Gazeas and Stepień 2008). With V958 Mon currently in its contact phase, it is far older than the Platais 6 stars.

5. Acknowledgements

The author wishes to thank Professor P. G. Niarchos for his careful readings, corrections, and valuable comments and suggestions on the draft version of this manuscript. This research was made possible through the use of the AAVSO Photometric All-Sky Survey (APASS), funded by the Robert Martin Ayers Sciences Fund. This research has made use of the SIMBAD database, operated at CDS, Strasbourg, France. Data from the Guo Shou Jing Telescope (the Large Sky Area Multi-Object Fiber Spectroscopic Telescope, LAMOST) were also used in this study. This telescope is a National Major Scientific Project built by the Chinese Academy of Sciences. Funding for the project has been provided by the National Development and Reform Commission. LAMOST is operated and managed by National Astronomical Observatories, Chinese Academy of Sciences.

References

Bilir, S., Karaali, S., and Tunçel, S. 2005, *Astron. Nachr.*, **326**, 321.

Bradstreet, D. H., and Stelman, D. P. 2002, *Bull. Amer. Astron. Soc.*, **34**, 1224.

Diethelm, R. 2011, *Inf. Bull. Var. Stars*, No. 5992, 1.

Gazeas, K., and Stepień, K. 2008, *Mon. Not. Roy. Astron. Soc*., **390**, 1577.

Henden, A. A., *et al.* 2014, AAVSO Photometric All-Sky Survey, data release 9 (http:www.aavso.org/apass).

Hoffman, D. I., Harrison, T. E., and McNamara, B. J. 2009, *Astron. J.*, **138**, 466.

Kafka, S. 2015, observations from the AAVSO International Database (https:/www.aavso.org/aavso-international-database).

Kharchenko, N. V., Piskunov, A. E., Roeser, S., Schilbach, E., and Scholz, R.-D. 2005, *Astron. Astrophys.*, **438**, 1163.

Kwee, K. K., and van Woerden, H. 1956, *Bull. Astron. Inst. Netherlands*, **12**, 327.

Lucy, L. B. 1968, *Astrophys. J.*, **151**, 1123.

Lucy, L. B., and Wilson, R. E. 1979, *Astrophys. J.*, **231**, 502.

Luo, A-Li, *et al.* 2015, *Res. Astron. Astrophys.*, **15**, 1095.

Mirametrics. 2015, Image Processing, Visualization, Data Analysis (http://www.mirametrics.com).

Mochnacki, S. W. 1981, *Astrophys. J.*, **245**, 650.
Nelson, R. H. 2011, *Inf. Bull. Var. Stars*, No. 6018, 1.
Otero, S. A., Wils, P., and Dubovsky, P. A. 2004, *Inf. Bull. Var. Stars*, No. 5570, 1.
Pecaut, M. J., and Mamajek, E. E. 2013, *Astrophys. J., Suppl. Ser.*, **208**, 9, (http://www.pas.rochester.edu/~emamajek/EEM_dwarf_UBVIJHK_colors_Teff.txt).
Qian, S., 2003, *Mon. Not. Roy. Astron. Soc.*, **342**, 1260.
Ruciński, S. M. 1969, *Acta Astron.*, **19**, 245.
Ruciński, S. M., and Duerbeck, H. W. 1997, *Publ. Astron. Soc. Pacific*, **109**, 1340.
Terrell, D., and Wilson, R. E. 2005, *Astrophys. Space Sci.*, **296**, 221.
Van Hamme, W. 1993, *Astron. J.*, **106**, 2096.
Van Hamme, W., and Wilson, R. E. 1998, *Bull. Amer. Astron. Soc.*, **30**, 1402.
Wilson, R. E. 1978, *Astrophys. J.*, **224**, 885.
Wilson, R. E., and Biermann, P. 1976, *Astron. Astrophys.*, **48**, 349.
Wilson, R. E., and Devinney, E. J. 1971, *Astrophys. J.*, **166**, 605.
Wozniak, P. R., *et al.* 2004, *Astron. J.*, **127**, 2436.
Wu, Z.-Y., Zhou, X., Ma, J., and Du, C.-H. 2009, *Mon. Not. Roy. Astron. Soc.*, **399**, 2146.
Zejda, M., Paunzen, E., Baumann, B., Mikulášek, Z., and Liška, J. 2012, *Astron. Astrophys.*, **548**, A97.